Chapter 2

Tropospheric O_3 distribution over the Indian Ocean during spring 1995 evaluated with a chemistry-climate model

Abstract

An analysis of tropospheric O_3 over the Indian Ocean during spring 1995 is presented based on O_3 soundings and results from the chemistry-general circulation model ECHAM (European Centre Hamburg Model). The ECHAM model is nudged towards actual meteorology using ECMWF analyses, to enable a direct comparison between model results and in situ observations. The model reproduces observed CO levels in different air mass categories. The model also reproduces the general tendencies and the diurnal variation in the observed surface pressure, although the amplitude of the diurnal variation in the amplitude is underestimated. The model simulates the general O_3 tendencies as seen in the sonde observations. Tropospheric O_3 profiles were characterized by low surface concentrations (< 10 ppbv), mid-tropospheric maxima (60-100 ppbv, between 700-250 hPa) and upper-tropospheric minima (< 20 ppbv, between 250-100 hPa). Large-scale upper tropospheric O_3 minima were caused by convective transport of O_3-depleted boundary layer air in the Inter Tropical Convergence Zone (ITCZ). Similarly, an upper tropospheric O_3 minimum was caused by cyclone Marlene south of the ITCZ. The mid-tropospheric O_3 maxima were caused by transport of polluted African air. The ECHAM model appears to overestimate surface O_3 levels, and does not reproduce the diurnal variations very well This could be related to unaccounted multiphase O_3 destruction mechanisms involving low level clouds and aerosols, and missing halogen chemistry

2.1   Introduction

During the Northern Hemisphere winter large scale cooling of the Tibetan Plateau is associated with the development of a high-pressure area over the Asian continent. In the boundary layer northeasterly outflow from this high-pressure area transports polluted air masses from Asia to the Indian Ocean and further towards the ITCZ (Inter Tropical Convergence Zone). The air masses can reach the central and south Indian Ocean, and the important question is to what extent the growing south-Asian pollutant emissions impact the composition of this relatively pristine atmosphere and the local radiation balance [Moorthy *et al.*, 1997; Rhoads *et al.*, 1997; Krishnamurty *et al.*, 1997; Lal *et al.*, 1998; Krishnamurti *et al.*, 1998a; Jayaraman *et al.*, 1998; Krishnamurti *et al.*, 1998b].

During transport in the marine boundary layer south of India the air masses encounter different cloud regimes, from low-level stratus to shallow convection and, ultimately, the deep convective clouds of the ITCZ. These different cloud regimes likely affect the chemical composition of the air masses and vise versa. Furthermore, the deep convective clouds in the ITCZ may penetrate the tropopause and inject pollutants directly into the stratosphere. Stratospheric air can also enter the troposphere, for example, near the subtropical jet stream. This large variety of meteorological and chemical processes makes the Indian Ocean a complex and interesting region to study. Unfortunately, to date there have been few measurements of chemical species over the Indian Ocean [Savoie *et al.*, 1987; Johnson *et al.*, 1990; Chester *et al.*, 1991; Baldy *et al.*, 1996]. To investigate these processes over the Indian Ocean in more detail a major measurement campaign, INDOEX (INDian Ocean EXperiment), will take place during the 1999 Indian winter monsoon.

As a preparation to INDOEX several pre-INDOEX ship cruises have been carried out. In this paper some results from the pre-INDOEX cruise of the NOAA R/V Malcolm-Baldrige are discussed. This cruise took place from March 21 (Julian Day 80, JD 80) to April 22 (JD 112), 1995, when the ship sailed from Durban, South Africa (29.8° S, 26.1° E) to Colombo, Sri Lanka (6.7° N, 79.6° E). During this cruise, near-surface measurements of chemical species were made continuously and O_3 sondes were launched approximately once per day. For a detailed discussion is referred to Rhoads *et al.* [1997] and Dickerson *et al.* [1998] for the surface data. In this paper a simulation for this period with the European Centre Hamburg Model [Roeckner *et al.*, 1996] extended with a chemistry scheme is presented and comparison is with the observations is made. This provides and ideal opportunity to evaluate the model in a tropical environment. A more detailed presentation of the model follows in section 2. The Newtonian relaxation technique is described in section 3, a brief summary of the measurements is presented in section 4, and a description of the trajectory model follows in section 5. The results are presented in section 6, starting with the discussion of the surface data, followed by the O_3 sonde results.

2.2 The ECHAM4 model

The General Circulation Model (GCM) used in this study is the 19 layer European Center Hamburg Model, version 4 (ECHAM4). In this study the T30 version of the model with a horizontal resolution of about 3.75° x 3.75° and a time resolution of 1800 seconds is used. The model uses a hybrid _-p coordinate system from the surface to 10 hPa. Average pressure levels relevant for the troposphere and lower stratosphere are 990, 970, 950, 900, 840, 760, 670, 580, 490, 400, 320, 250, 190, 140, 100 and 75 hPa, referring to approximate mid-layer altitudes of 0.03, 0.14, 0.38, 0.78, 1.4, 2.1, 3.1, 4.2, 5.6, 7.0, 8.6, 10.2, 11.9, 13.8, 15.9 and 18.0 km above the surface. Tracer transport is calculated using a semi-Lagrangian advection scheme [Rasch and Williamson, 1990]. Vertical transports are included through parameterizations of vertical diffusion and convection [Roeckner *et al.*, 1996; Tiedtke, 1989]. An elaborate description of ECHAM4 and the simulated climate can be found in Roeckner *et al.* [1995], Chen and Roeckner [1996], and Haskins *et al.* [1995]. In this study, ECHAM4 is coupled to a tropospheric chemistry model that considers background CH_4-CO-NO_x-HO_x chemistry, emissions of NO and CO, dry deposition of O_3, NO_2, HNO_3 and H_2O_2, and wet deposition of HNO_3 and H_2O_2. Concentration changes due to chemical reactions are calculated explicitly for all species by means of an Eulerian Backward Iterative (EBI) scheme. A detailed description and analysis of the coupled chemistry GCM is given in Roelofs and Lelieveld [1995, 1997].

The model considers a biomass-burning source for NO of 6 Tg N yr^{-1} and for CO of 700 Tg CO yr^{-1}, distributed according to Hao and Liu [1994]. NO emissions from soils and from lightning play an additional role in the tropical tropospheric O_3 budget. These sources in the model are 5.5 Tg N yr^{-1}, distributed according to Yienger and Levy [1995], and 5 Tg N yr^{-1}, parameterized according to Price and Rind [1992]. Further, the model considers global NO emissions from fossil fuel burning (21 Tg N yr^{-1}; Benkovitz *et al.* [1996]), and CO emissions from fossil fuel burning (450 Tg CO yr^{-1}), vegetation (100 Tg CO yr^{-1}), formation from natural (280 Tg CO yr^{-1}) and antropogenic (300 Tg CO yr^{-1}) higher hydrocarbons, oceans (40 Tg CO yr^{-1}) and wildfires (30 Tg CO yr^{-1}). CO emissions are distributed according to Lelieveld and Van Dorland [1995]. The total NO and CO emissions considered in the model are 37.5 Tg NO yr^{-1} and 1900 Tg CO yr^{-1}, consistent with IPCC [1994]. In view of the relatively long lifetime of CH_4, the CH_4 surface concentrations are prescribed.

The parameterization for dry deposition of O_3, NO_x, and HNO_3 is described in Ganzeveld and Lelieveld [1995, 1998]. It derives aerodynamic and stomatal resistances directly from parameters calculated by ECHAM4. The wet scavenging of HNO_3 and H_2O_2 is calculated using the large scale and convective cloud and precipitation properties calculated on-line by the climate model as described in Roelofs and Lelieveld [1995, 1997]. Stratospheric O_3 concentrations are prescribed between 1 to 2 model layers above the tropopause up to 10 hPa, the top level of the GCM. Transports of O_3 across the tropopause depend directly on the air motions simulated by the GCM. The simulated tropopause is marked by a potential vorticity of $3.5 \cdot 10^{-6}$ K m^2 kg^{-1} s^{-1} poleward of 20° latitude [Hoerling *et al.*, 1993], and by a -2 K km^{-1} temperature lapse rate equatorward of 20° latitude.

The model realistically represents the seasonal variability of the O_3 photochemical production and of O_3 transport from the stratosphere [Roelofs and Lelieveld, 1995 and 1997]. Surface O_3 concentrations as measured in remote and relatively clean conditions are also reproduced, but the model appears to underestimate O_3

concentrations in some polluted regions due to the neglect of higher hydrocarbon chemistry [Roelofs *et al.*, 1997].

2.3   Newtonian Relaxation

In this study a four-dimensional assimilation technique (nudging) is used to relax the ECHAM4 model towards an observed state, in this case ECMWF analyses. Originally, this technique was used to improve numerical weather prediction by nudging the model towards observations during a spinup period, after which the model produced a prediction. Nowadays, nudging is a very useful technique for validation of cloud and chemistry schemes in GCMs for which long time series of measurements are not available. The technique can be used to adjust the ECHAM4 model towards an observed state for a longer period of time. Observations made during that period can then be compared directly with the model. A more detailed description of the Newtonian relaxation is given by Jeuken *et al.* [1996].

The model is nudged toward the observed state by the addition of a non-physical relaxation term to the model equations:

$$\frac{\partial X}{\partial t} = F_m(X) + G(X_{obs}-X) \qquad (1)$$

With X representing a prognostic model variable, F_m is the model forcing, $(X_{obs}-X)$ represents the difference between model state and observed state and G is a relaxation coefficient (s^{-1}). At every time step the model is relaxed towards ECMWF analyses. Since the timestep of the model does not correspond to the availability of the analysis in the data archive (6 hours), the ECMWF data are interpolated to match the model time step. Such an interpolation was proposed by Brill *et al.* [1996].

The divergence, vorticity, temperature, surface pressure and sea-surface temperature are nudged as in Jeuken *et al.* [1996]. The choice of the relaxation coefficient G is rather arbitrary. However, G cannot be chosen too small as the observations will have little effect on the model output. On the other hand, if G is too large the model will be nudged too strongly to the observed field and possible imbalances can be amplified. The value of G can also have a spatial distribution because the accuracy of the observations has a wide range [Hoke and Anthes, 1976]. More accurate observations should have more influence on the model than less accurate observations. This can be achieved by using the adjoint of the numerical model [Zou *et al.*, 1992], which calculates G for each gridpoint separately. The ECMWF analysis is already adjusted towards numerous observations using an extensive four-dimensional data assimilation scheme [Heckley, 1992]. Furthermore, the model output is only weakly dependent on the choice of G in the extratropics [Jeuken *et al.*, 1996; Krishnamurty *et al.*, 1991], so the relaxation coefficients can be chosen to have a constant value (experiment 5 from Jeuken *et al.* [1996], given in Table 1).

| *Coefficient*	G_T	G_D	G_{Vo}	G_{Spr}
value	1.10^{-5}	$0.5.10^{-4}$	1.10^{-4}	1.10^{-4}

Table 1. Relaxation coefficients applied in the ECHAM4 model. G_T, G_D, G_{V_o} and G_{spr} are the relaxation coefficients (s^{-1}) for temperature, divergence, vorticity and surface pressure, respectively.

The humidity field is not nudged. Using the humidity field from the ECMWF analysis as a nudging variable would require a different approach. The modelled humidity field is strongly dependent on the parameterizations of, for example, clouds, ice, snow, rainfall, etc. The dependence on the parameterizations should be taken into account if the ECMWF humidity fields are used as errors could be created by the different parameterizations in the ECMWF and ECHAM4 models. A method to nudge the humidity field is proposed by Krishnamurty *et al.* [1988, 1991]. This method uses observed rainfall rates to calculate a corresponding humidity field with the use of an inverse modelling technique. However, this kind of inverse modelling is currently not available for the ECHAM4 model. It is also important to note that the ECMWF data that is used in this study do account for the effects of the humidity on the circulation in the tropics, so that these effects are indirectly included in the nudging of the ECHAM model. Therefore, it can be expected that including the humidity field in the nudging process does not have a large effect on the model output. A comparison between observed humidity profiles and the model shows that the model indeed is capable of simulating the observed profiles very well (unpublished data). It can also be noted that the aim of the nudging is to reproduce the observed circulation patterns without affecting the physical properties of the model. To what extent the nudging affects these properties is difficult to say, but, the more model parameters are nudged towards the ECMWF analysis, the mode likely it becomes that one is not comparing the ECHAM model with the observations but the ECMWF model.

For the current model simulations ECHAM4 was integrated without nudging for the period of September to February to allow time for the spin-up of tracer fields. After the spinup period Newtonian relaxation was applied for the period from 16 March to 30 April 1995. Although there was also a spinup because of the onset of the nudging procedure, the spinup period turned out to be less than a day and was therefor not important for the model output.

2.4 Measurements

On March 21, 1995, the R/V Malcolm-Baldrige departed from Durban, sailing toward Sri Lanka following the cruise track shown in Figure 1. During this voyage near-surface measurements of trace gases, e.g. CO, O_3, NO_x, aerosols and of meteorological variables were made. For a detailed description of these measurements see Rhoads *et al.* [1997] and Dickerson *et al.* [1998]. Rhoads *et al.* [1997] show that along the cruise track from south to north four distinct meteorological air masses or regimes were encountered, i.e. southern hemisphere marine extratropical air (SHmX), southern hemisphere marine equatorial air (SHmE), northern hemisphere marine equatorial air (NHmE) and northern hemisphere continental tropical air (NHcT). These different regimes are distinguished by sharp increases in the surface trace gas and aerosol concentrations measured on days 91, 101, and 107 [Figure 2, Rhoads *et al.*, 1997].
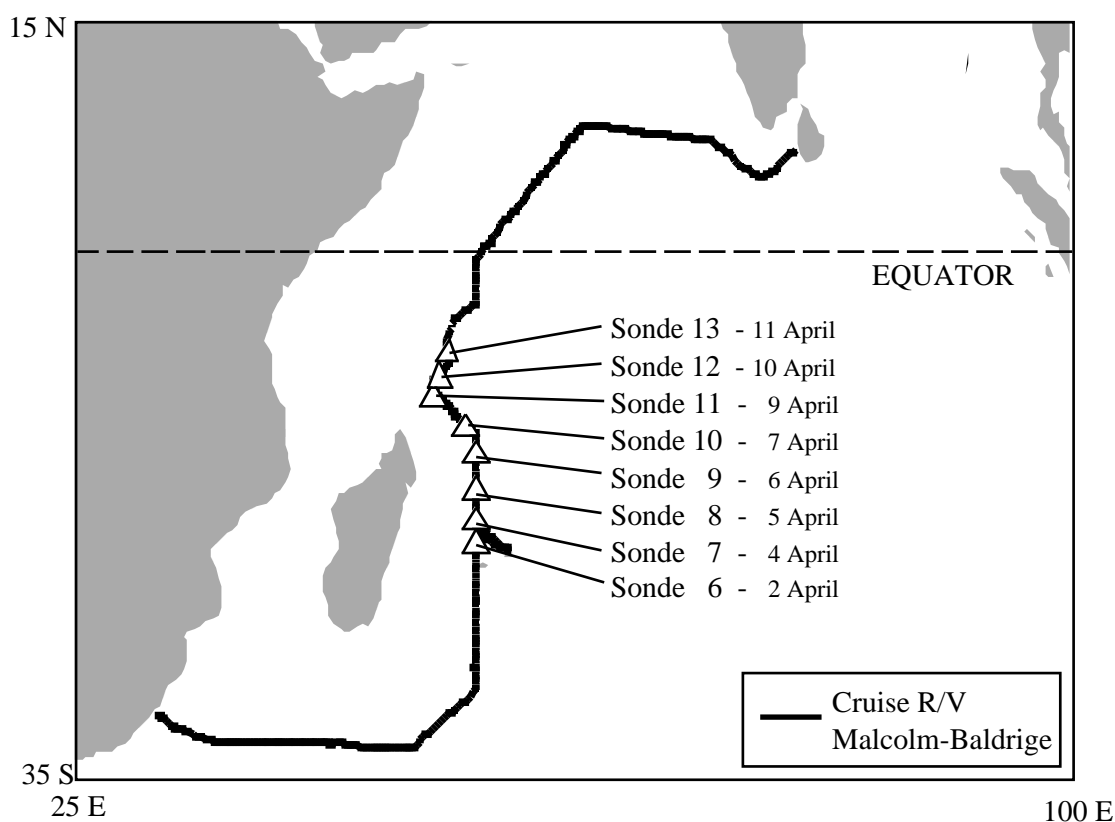
Figure 1. The track of the research vessel Malcolm-Baldrige. The triangles show the sites and dates were the sondes were launched. The campaign started on March 12, 1995, in Durban, South Africa, and ended on April 22, 1995, in Colombo, Sri Lanka.

O_3, humidity and temperature measurements aloft were obtained using balloon-borne electrochemical concentration cell (ECC) O_3 sondes (Model 1z, En-Sci Corp., Boulder, Colorado) coupled to Väisälä radiosondes (Model RS80, Väisälä USA, Woburn, Massachusetts). The Väisälä sensors for temperature, pressure and humidity measurements were factory calibrated and have reported accuracy's of 0.3 °C, 0.5 hPa and 2 % respectively.

The O_3 sensor has an accuracy of $\pm$ 7 % in the troposphere, with a detection limit of 1-2 ppbv [Komhyr *et al.*, 1995]. The uncertainty at concentrations less than 10 ppbv is of the order of 10 %. The reported accuracies assume a constant background current correction determined on deck prior to launch. The sondes were typically launched in the early afternoon at intervals of approximately 2 degrees of latitude. The sondes and a UV absorption instrument made simultaneous measurements for a few minutes prior to most launches. During these periods the signals tracked well together with the sonde measurements averaging 2.3 ppbv higher than the UV absorption instrument. The observed differences between the two signals are within the combined uncertainty of the two detectors.

2.5   Trajectory model

Trajectory analyses were performed in order to determine the origin of the air masses of interest. The trajectory model used in this study is the KNMI (Royal Netherlands Meteorological Institute) trajectory model [Scheele *et al.*, 1996]. Three-dimensional ECMWF first-guess (6 hour forecast) wind fields are used to calculate the displacement of an air parcel for each model time step of the trajectory model. The use of first-guess data instead of analyses ensures that the wind fields and mass distribution fields are in physical balance. The first-guess wind data are available at 31, hybrid σ-p, model levels and at a horizontal resolution of T213 (approximately 0.5°x0.5°).

Since the gridpoints and times of these wind data generally do not coincide with those of the points for which the back trajectories are determined, interpolation in space and time is required. The spatial interpolation is linear in the horizontal direction and linear with log(p) in the vertical direction. A quadratic interpolation in time is applied to convert the 6-hour wind field data to 1-hour data, which matches the time step of the trajectory integration. The calculation of a new trajectory position is performed iteratively until the difference between subsequent estimated end points is less than 300 m in the horizontal and less than 0.0001 times the pressure in the vertical direction.

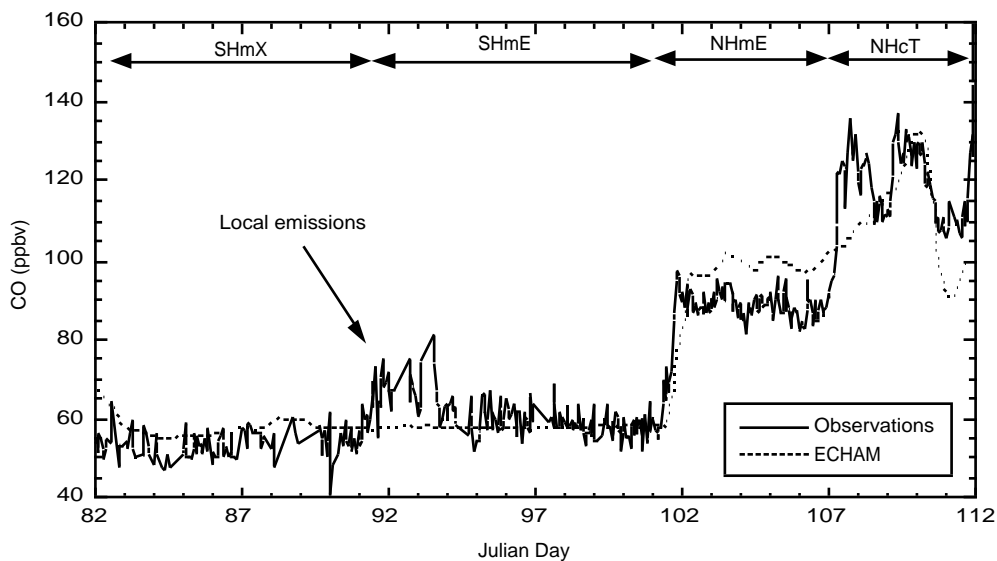## 2.6   Results

2.6.1   Surface data

A comparison is made between model and measurements for CO, O_3 and the surface pressure. Since the location and time of the observations generally do not coincide with those of the ECHAM4 model, interpolation of the model output in space and time is performed for both sonde and surface observations. Tables 2 and 3 list the average CO and O_3 concentrations for the four different air mass regimes as indicated in section 4.

	SHmX	*SHmE*	*NHmE*	*NHcT*
CO measured	54.1 ($\pm$ 4.0)	59.3 ($\pm$ 3.7)	89.0 ($\pm$ 3.3)	120.4 ($\pm$ 9.8)
CO ECHAM4	55.0 ($\pm$ 2.7)	58.7 ($\pm$ 0.9)	96.3 ($\pm$ 7.6)	110.7 ($\pm$ 12.5)

Table 2. Average measured and modelled CO concentrations (ppbv) at the surface for the four different air mass regimes. Standard deviations are shown in brackets. Measurements are from Rhoads *et al.* [1997].

	SHmX	*SHmE*	*NHmE*	*NHcT*
O_3 measured	17.0 (± 1.8)	11.5 (±2.5)	7.5 (± 1.2)	15.7 (± 2.9)
O_3 ECHAM4	20.8 (± 3.2)	16.9 (± 2.0)	14.1 (± 1.0)	24.6 (± 4.7)

Table 3. Average measured and modelled O_3 mixing ratios (ppbv) at the surface for the four different air mass regimes. Standard deviations are shown in brackets. Measurements are from Rhoads *et al.* [1997]. Mixing ratios in ppbv.


Figure 2. Comparison between measured and modelled CO. The observations are shown by the solid line, the model results by the dashed line. The arrows at the top of show the position of the different types of air (see section 4).

From Figure 2 and Table 2 it can be seen that the simulated CO concentrations of both the SHmX air mass and the SHmE air mass agree well with the measurements (Julian days 81 to 91.5). The air mass encountered between JD 92 and JD 94 is probably affected by local emissions [Rhoads *et al.*, 1997]. The measured CO concentrations for the southern hemisphere air masses can be considered to represent background CO concentrations as they are far away from major pollution areas. Furthermore, according to Figure 2, the model calculates the ITCZ at the right location and time, as indicated by the increase in CO concentration on JD 102. On average, the model produces higher concentrations for the NHmE air and lower concentrations for the NHcT air, but observations and modelled concentrations are still within the modelled standard deviation (see Table 2). The observations show two distinct maxima in the CO concentrations between JD 107 and 111, with peak values of about 140 ppbv. These maxima are related to the vicinity of the Indian

subcontinent [Rhoads *et al.*, 1997]. The model captures only the second maximum, which is probably related to the relatively low resolution of the model. However, the maximum modelled concentration for the second maximum is the same as the observed one. As for the timing of the change from the NHmE mass to the NHcT air mass, the changes in the model are again at the right location and time (Julian Day 107). This can be seen even better in Figure 3 for O_3. Taking the large standard deviations into account, modelled and observed concentrations seem to compare well.

The results for O_3 are shown Figure 3 and the average concentrations of the different types of air are given in Table 3. The most striking features of Figure 3 are the low O_3 concentrations (7.5 ppbv on average) for the NHmE air. Similar or even lower concentrations have been measured in the equatorial Pacific [Routhier *et al.*, 1980; Fishman *et al.*, 1983; Piotrowicz *et al.*, 1986; Piotrowicz *et al.*, 1991; Singh *et al.*, 1996; Kley *et al.*, 1996]. Such low O_3 concentrations appear to be a common feature of remote equatorial marine environments. They are associated with clean, NO_x-depleted O_3 destruction conditions, although the exact mechanisms by which the very low concentrations are caused are still a subject of debate [Singh *et al.*, 1996].
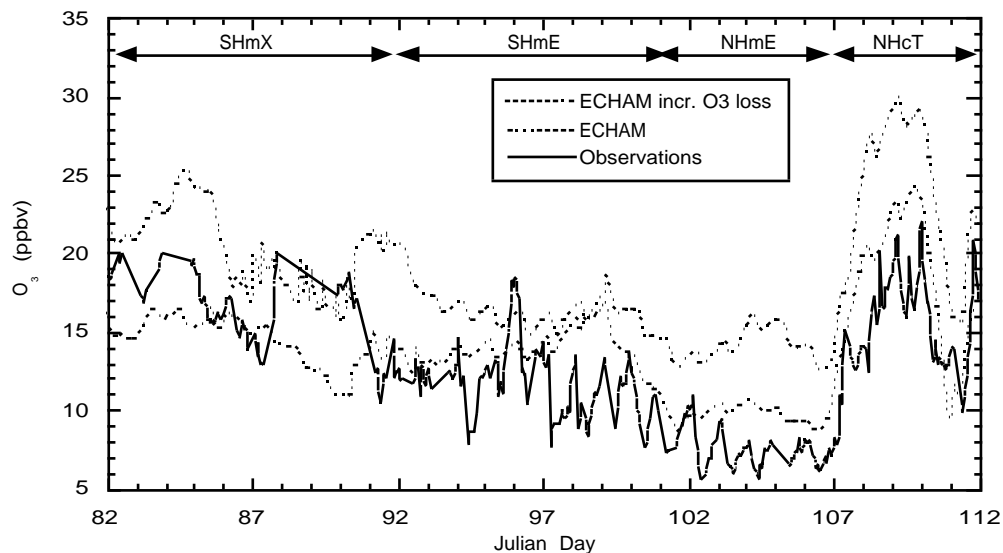
Figure 3. As Figure 2 but for O_3. The thick dashed line shows the model calculated O_3 for which the O_3 destruction through the reaction $O(^1D) + H_2O$ in the marine boundary layer has been doubled over the Indian Ocean.

Figure 3 shows that the model is capable of producing the same observed latitudinal trend, but it produces higher O_3 concentrations during most of the period, except for JD 88-91. Note that for this period only a few observations were available. The mean difference between observed O_3 and modelled O_3 is 6 ppbv (± 3 ppbv). Figure 4 shows the observed and modelled NO_x concentrations. Observations were only available for the period after JD 101. The uncertainty in NO_x is 20 pptv while the average NO concentration is 6 pptv. Although the modelled NO_x concentrations are generally lower than observed, concentrations in both observations and model indicate that O_3 production is very slow. Therefore, the model overestimation of O_3 in the Indian Ocean boundary layer is not caused by an overestimation of photochemical

O_3 production, but rather by some O_3 destruction mechanism that is not well represented by the model. It is not likely that the O_3 mismatch is caused by a problem in the model representation of transport and mixing. In that case a similar problem would arise with CO, which is not manifest from Figure 2. A possible explanation could be the neglect of multiphase chemical processes in low-level clouds of aqueous aerosols.
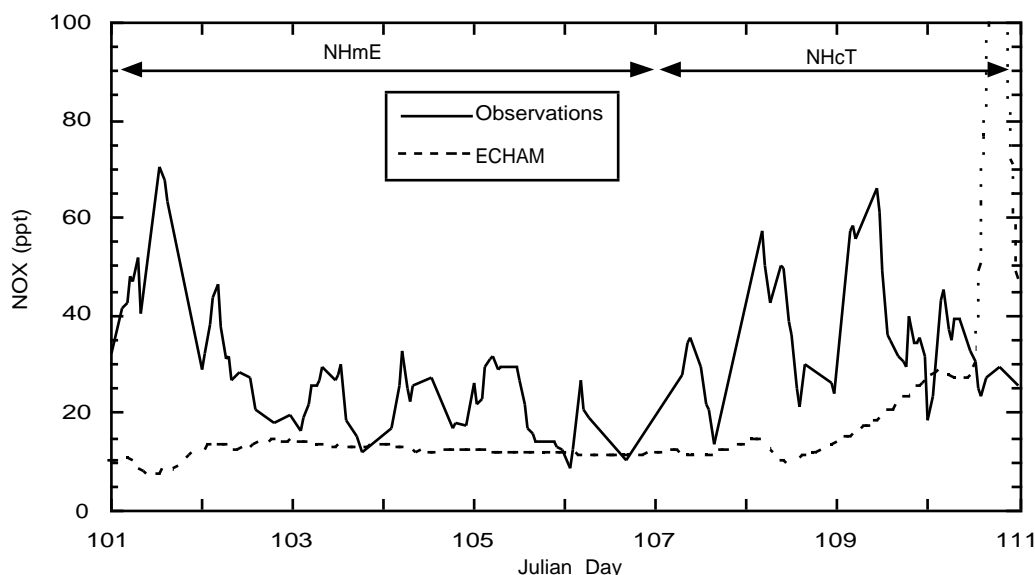

Figure 4. Same as Figure 2 but for NO_x, for the last ten days of the campaign (Julian day 101-111).

Cloud and aerosol chemistry could lead to enhanced destruction of peroxy radicals that form O_3, to O_3-loss in the aqueous phase [Lelieveld and Crutzen, 1990], or to the release of reactive halogens from dissolved sea salt and subsequent O_3 destruction [Vogt *et al.*, 1996]. A first estimate has been obtained by increasing the O_3 destruction in the marine boundary layer of the model. The reaction rate of $O(^1D)$ + H_2O is multiplied by a factor of 2. Figure 3 shows that this strongly improves the agreement.

A remarkable feature, which can be seen in Figure 3, was the strong diurnal cycle present in the O_3 measurements (JD 93-107). This diurnal cycle could have been caused by photochemical O_3 destruction during the day, and nighttime replenishment by mixing. A diurnal cycle with a minimum during the day is discernible in the model results (JD 93-107), consistent with the measurements, but the amplitude is smaller then the observed one. The observed amplitude of the diurnal cycle has a value of about 4 ppbv while the amplitude in the model is about 0.5-1.0 ppbv. Rhoads *et al.* [1997] noted that O_3 destruction started after sunrise and that the lowest O_3 levels were found just after solar noon. The model also shows a minimum during daytime caused by daytime photochemical destruction of O_3, mostly through photodissociation of O_3 and the subsequent reactions of $O(^1D)$ with H_2O. Enhanced daytime photochemical O_3 destruction would be consistent with the mechanisms

proposed by Lelieveld and Crutzen [1990], Vogt *et al.* [1996] or Dickerson *et al.* [1998], which will be studied in greater detail in future.
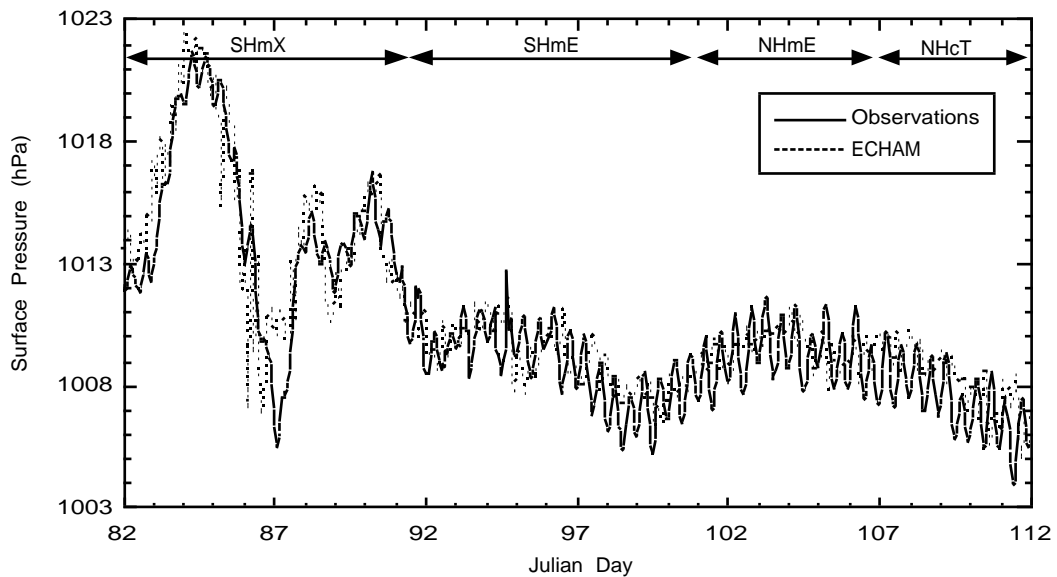

Figure 5. As Figure 2 but for the surface pressure.

In Figure 5 a comparison is made between measured and modelled surface pressure, which agree very well. The maxima on Julian Days 84, 88 and 91 and the minima on days 84 and 87 are reproduced by the model, as well as the overall tendency for the period after Julian Day 92. The model also produces the semi-diurnal variability although the modelled amplitude (0.5-1.0 hPa) is slightly smaller than the observed one (1.5 hPa). This is most clearly shown for the period after JD95. This semi-diurnal cycle of the surface pressure is consistent with the findings of Hsu and Hoskins [1989] who found that such fluctuations in the ECMWF analyses are consistent with tidal movements. Although the surface pressure is a nudged variable, a good agreement between measured and modelled surface pressure is not trivial. The ECMWF analyses in this region are based on only few observations so that uncertainties in the model performance can be expected. However, according to Figure 5 this is not the case for the surface pressure.
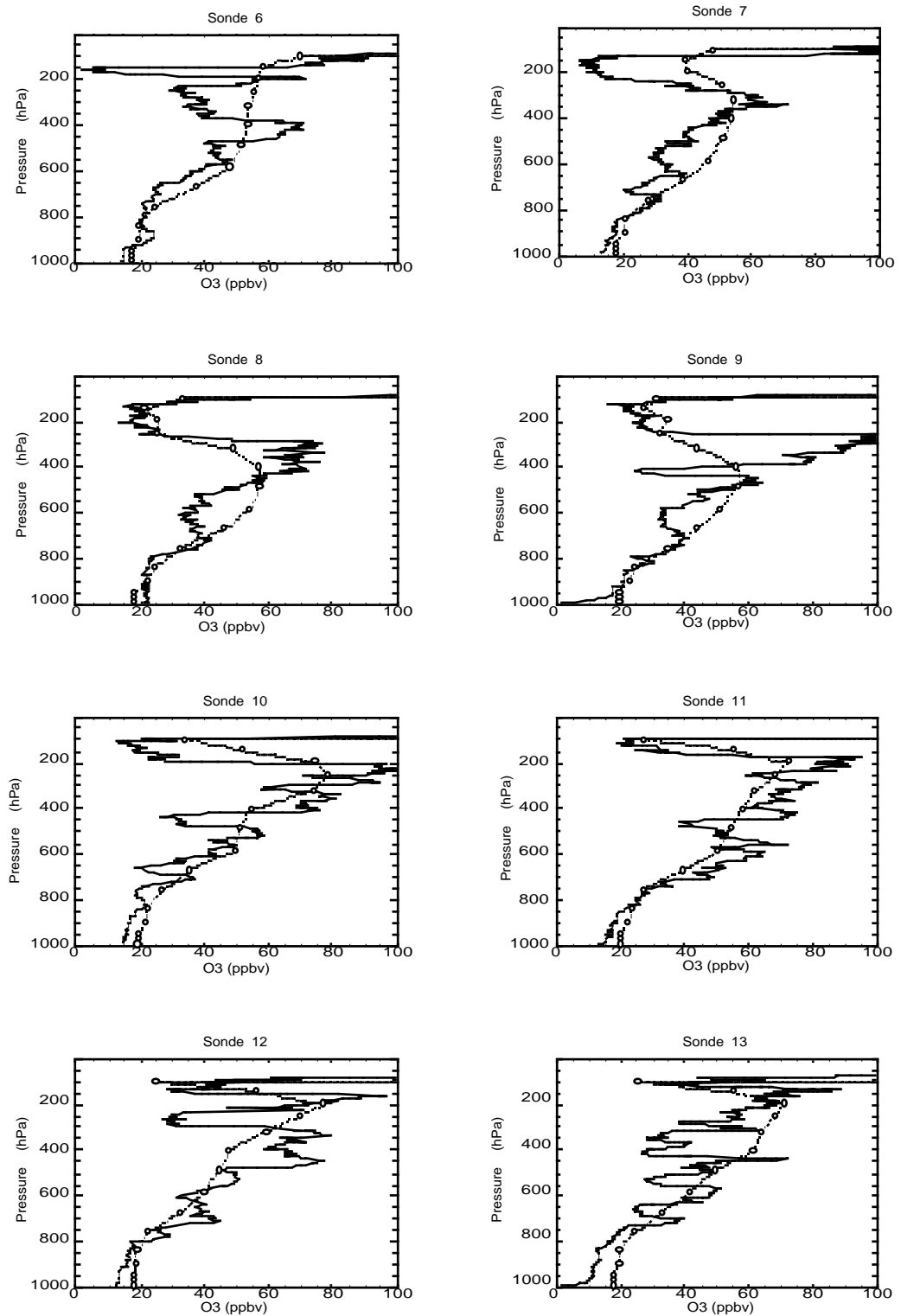
2.6.2 O_3 Sondes

Figure 6 shows the O_3 contour plot for all sondes. Two remarkable features in the upper air data are the relative ozone minimum at 175 hPa, near 18S, and O_3 maximum at 300 hPa, around 13S. The minimum was observed over the course of 5 days from four consecutive sondes. These upper tropospheric layers showed ozone levels ranging from 20 to less than 10 ppbv. Although the region of minimum ozone is not associated with high relative humidity, large-scale rising motion may have lifted low ozone air up from the boundary layer and lower free troposphere. Mixing ratios at the minimum are in line with those observed in the lower free troposphere

and a more humid layer appears at the bottom of low ozone strata in several of the profiles. The region of high ozone coincides with quite low relative humidity (~5%), suggesting that the air is stratospheric in origin.
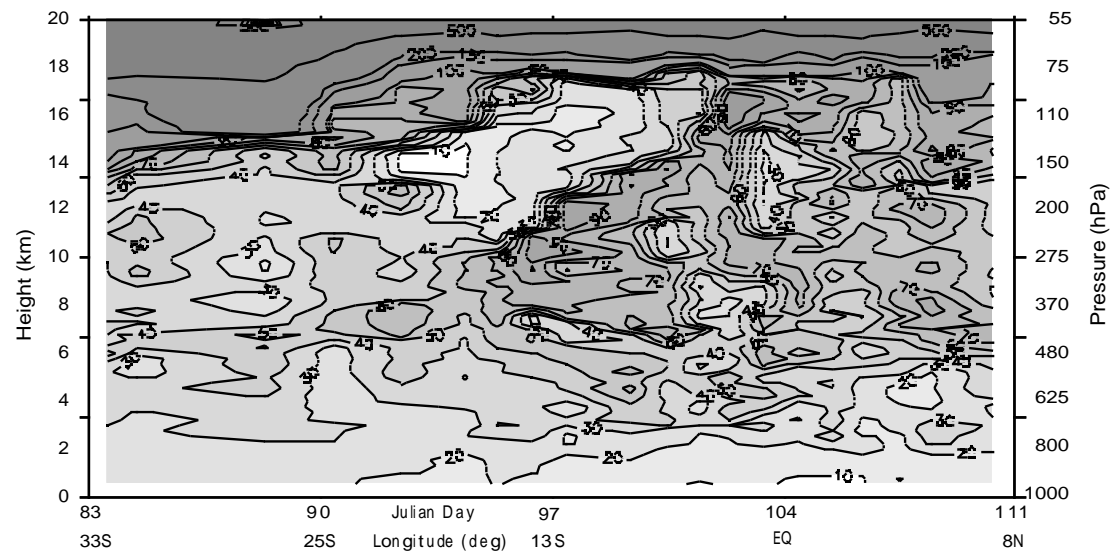

Figure 6. Latitude/time versus height contour plot for O_3 for all sonde observations performed during the 1995 campaign. Contour values given in ppbv.

Figure 7 shows the comparison between eight O_3 soundings and the ECHAM4 model results. The positions of the sondes as well as the dates at which they were released can be seen in Figure 1. The 8 sondes show some common features. At the surface the O_3 concentrations are relatively low due to photochemical destruction. The O_3 concentrations increase with height, and the

Figure 7. Comparison of eight O_3 sondes and the modelled O_3 profiles. Location and time of release of the sondes are given in Figure 1. The observations are denoted by the dashed lines, the model output by the solid lines.

highest O$_3$ levels are found between 400 and 200 hPa (7-12 km). Directly above these maxima very distinct minima appear. The ECHAM4 model is capable of capturing most of these general features, i.e. the low surface concentrations, the gradual increase of O$_3$ concentrations with height and the upper tropospheric minimum. The model also captures the tropopause height, indicated by the sharp increase in O$_3$ concentrations above 100 hPa.
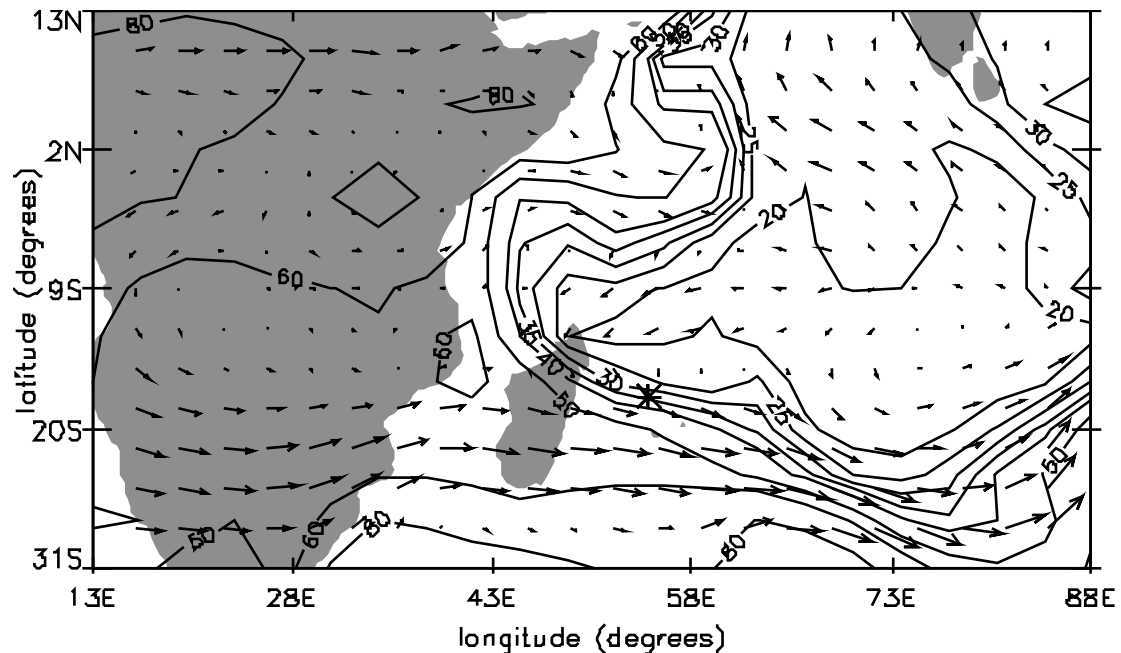

Figure 8. Simulated O$_3$ concentrations (ppbv) for April 4 at 05:00 UTC at an altitude of 190 hPa. Also shown are the wind fields (arrow length in arbitrary units). The asterisk at 55E, 18 S denotes the position of the ship.

The upper tropospheric minimum is the result of the ITCZ outflow at this height. The convective cells at the ITCZ ventilate boundary layer air all the way up to the tropopause. The boundary layer air has O$_3$ concentrations of about 20 ppbv or less, and in some cases the upper tropospheric minima also approach 20 ppbv. Figure 8 shows the model results at the 190 hPa level on April 4. A distinct minimum covers the entire Indian Ocean. To the west, the O$_3$ depleted air is bordered by O$_3$ rich continental African air. To the south the minimum is delimited by the subtropical jet, which transports O$_3$ rich African air eastward. The subtropical jet is also associated with transport of stratospheric air into the troposphere.
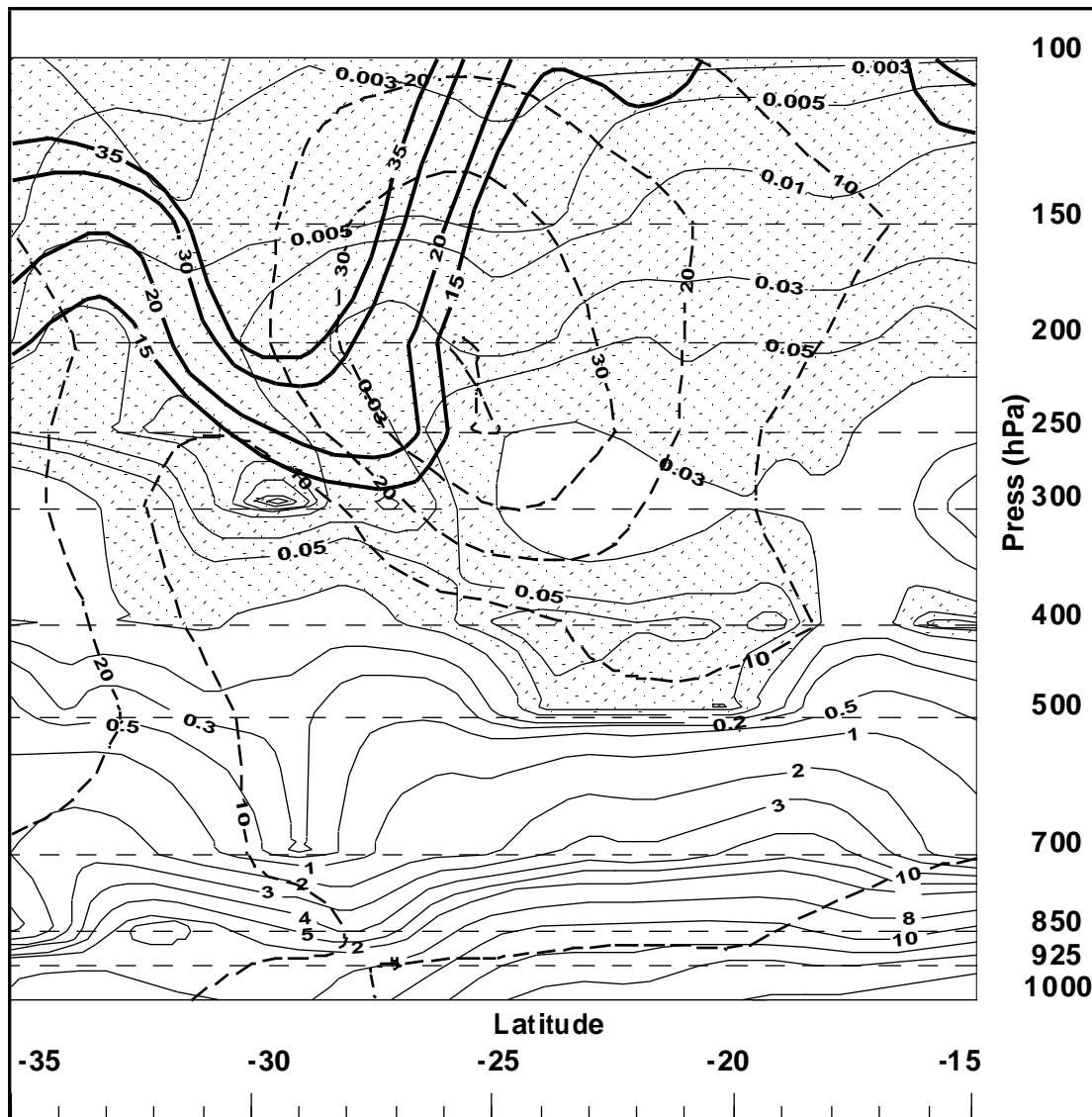
Figure 9: ECMWF analyses at 61°E on April 3 (18:00 UTC). *Thin solid line*: specific humidity (g/kg), with shaded regions showing air dryer than 0.1 g/kg. *Thick dashed line*: zonal wind velocity (m/s). *Thick solid line*: potential vorticity (0.1PVU).

This is illustrated in Figure 9, which shows the ECMWF analysis at 61° E on April 3. At a height between 300 and 100 hPa (10-18 km, near 30° S) a tongue of high potential vorticity descents into the troposphere. At this location stratospheric O_3 was transported into the troposphere. At the locations where the O_3 depleted marine air and O_3 rich continental air meet, sharp gradients occur (Figure 8).
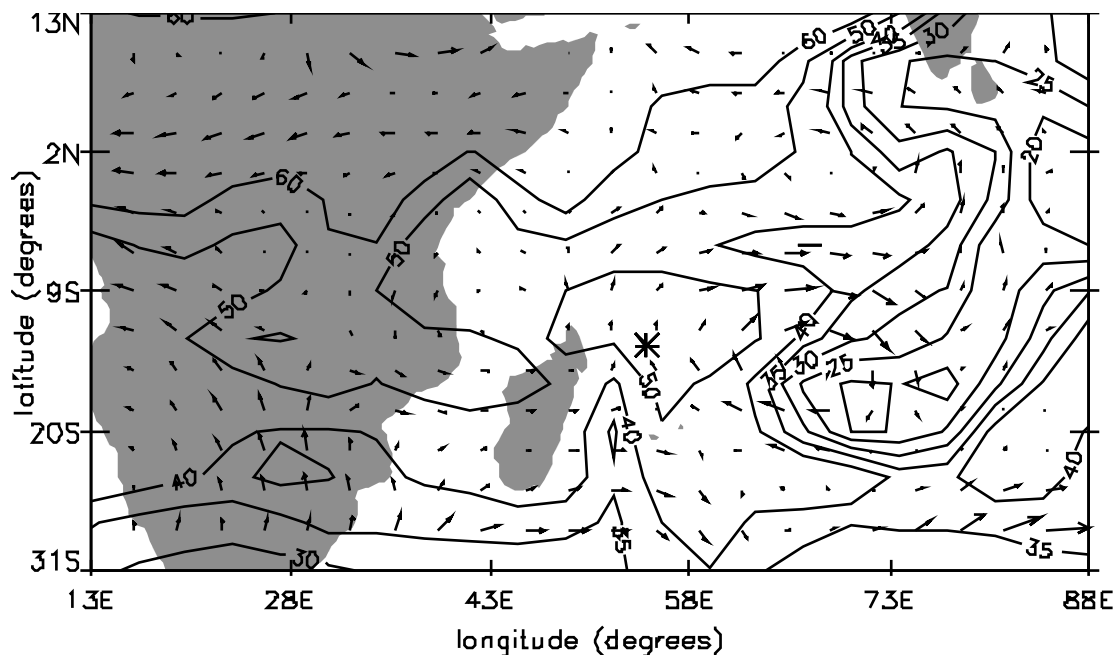
**Figure 10.** As Figure 8 but for April 6 at 07:00 UTC at an altitude of 580 hPa.

Figure 10 shows that the mid-troposphere is generally O_3-richer than the marine boundary layer as well as the upper troposphere. Relatively low O_3 levels occur in a relative small corridor at about 75 E. It appears that this area is affected by cyclone Marlene which was present at 65° E, 15 S°.
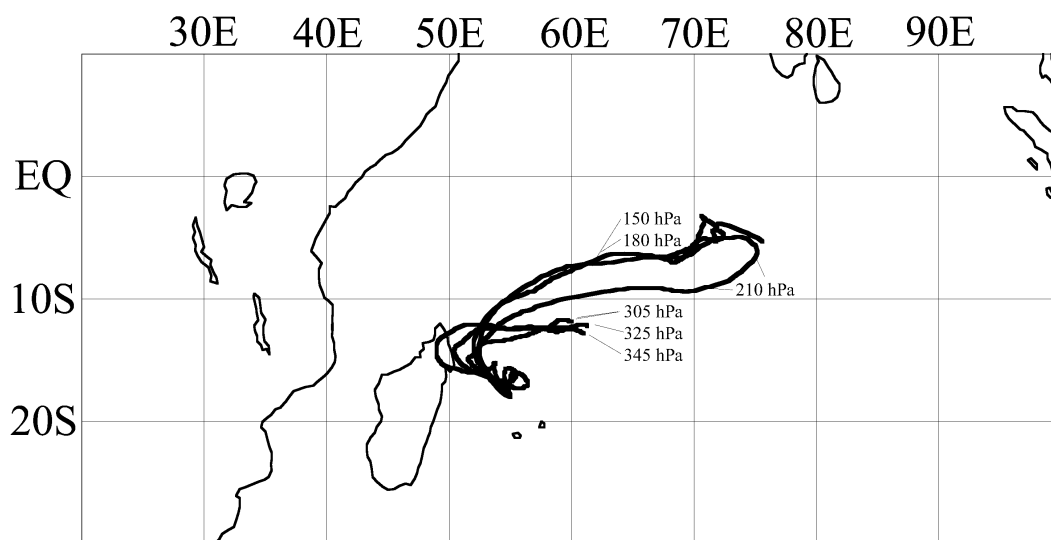
Figure 11: Back trajectories from April 4 (10:00 UTC) to March 30 (10:00 UTC), starting at 55E, 18.02S. The trajectories are marked by their starting pressure, i.e. 150, 180, 210, 305, 325 and 345 hPa.

To investigate the origin of the high tropospheric O_3 minimum observed in sonde 7 (April 4), a trajectory study was performed. Figure 11 shows 5-day back trajectories starting at 150, 180 and 210 hPa, representing the air in the O_3 minimum, and at 305,

325 and 345 hPa, representing the air mass just below the minimum. The air in the O_3 minimum clearly originates from the east, where O_3-depleted air is present according to the model (Figure 8). Figure 12 shows the vertical displacement of the trajectories. As the trajectory model is not capable of capturing individual convective cells, the trajectories mainly remain in the upper troposphere. The trajectory at 210 hPa, however, originates from the boundary layer. This can be traced back to the tropical cyclone Marlene. The strong vertical motion is caused by organized upward flow in cyclone Marlene.
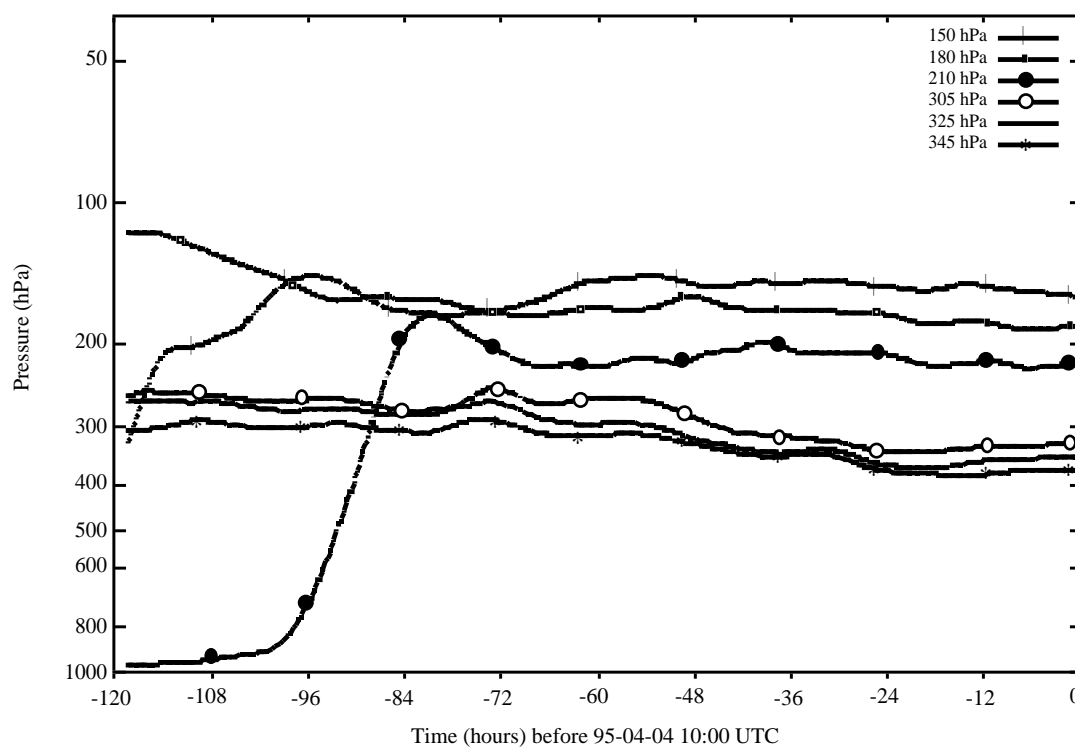

Figure 12: Pressure evolution with time of back trajectories from April 4 (10:00 UTC) to March 30 (10:00 UTC). On April 4 the trajectories started at the following pressure levels: 150, 180, 210, 305, 315 and 345 hPa.

The model is generally capable of matching the observed O_3 minimum in the upper troposphere. However, for sonde 6 the model cannot capture the minimum. The reason is probably that the vertical extent of the minimum is comparable to the size of a gridbox, which makes it difficult to model. For sonde 7 the model does produce a minimum, but the modelled O_3 concentrations are too high. According to Figure 8, the location of the sonde at that moment is within a sharp O_3 gradient. A relatively small shift within this gradient can strongly influence calculated O_3 concentrations, especially considering the size of the model grid cells.

Due to the coarse vertical resolution the model cannot capture most of the small-scale features apparent in the observations. The model does reproduce the general shape of the O_3 profiles although it somewhat underestimates the mid-tropospheric O_3 maximum. This might be related to the absence of higher hydrocarbon chemistry, which can cause an increase in the O_3 concentrations of 10-20 ppbv in air that is affected by pollution emissions [Roelofs *et al.*, 1997]. The model does not reproduce

the O_3 maximum at 300 hPa observed from sonde 9. Back trajectories calculated for this location (Figure 13) show that the air above 160 hPa originates from the east while below 180 hPa the air originates from the west. If the back-trajectories are representative for the meteorological situation, O_3 rich air would be found in the observations of sonde 9 at 180 and 200 hPa. This is definitely not the case at 180 and 200 hPa as can be seen in Figure 4. The inconsistency between the observed profile and the back-trajectories (the back-trajectories start close to each other but have a completely different origin) is indicative of the uncertainties involved in reproducing the meteorological situation. The resolution of the ECHAM model is much lower than that of the trajectory model, and it cannot be expected that ECHAM4 reproduces such small-scale meteorological features.
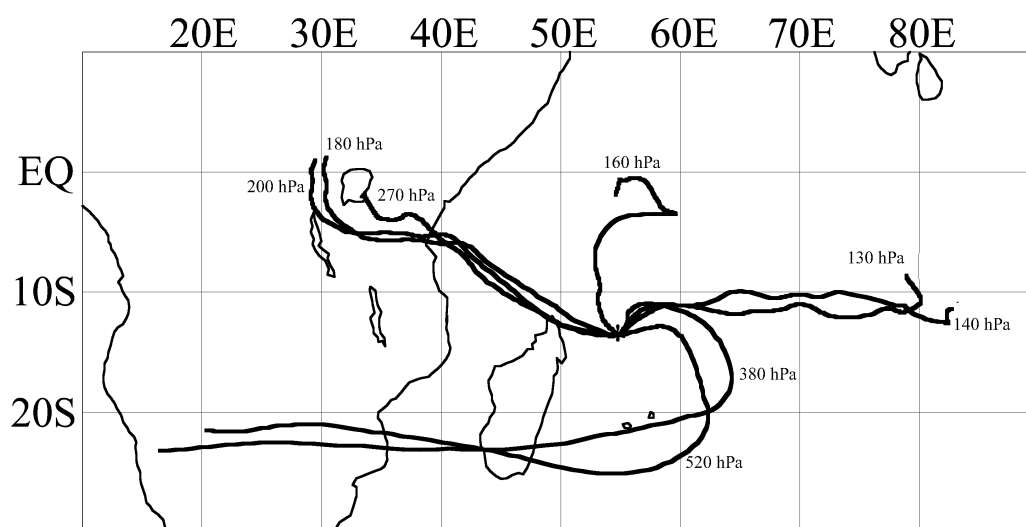
Figure 13: Back trajectories from April 6 (10:00 UTC) to April 1 (10:00 UTC), starting at 55E, 13.56S. The trajectories are marked by their starting pressure, i.e. 130, 140, 160, 180, 200, 270, 380 and 520 hPa. The trajectories starting at 380 and 520 hPa are representative for all trajectories starting at pressure levels between 380 and

At lower levels (520-380 hPa) the trajectories for sonde 9 are very consistent. They all originate from the southern part of Africa. The trajectories move eastward over the southern tip of Madagascar and then curve around to the measurement site. The trajectories suggest transport of O_3 rich African air. This is consistent with the findings of Piketh *et al.* (1996), Tyson *et al.* (1996), Tyson *et al.* (1997) and Bremaud *et al.* (1998), who all reported transport of polluted (O_3 rich) southern African air onto the southern Indian Ocean. The ECHAM4 model reproduces the observed O_3 concentrations at this altitude, and Figure 10 shows south-easterly winds around 60° E, 15 S, consistent with the curved trajectories at this location. In general, stratosphere-troposphere transports are small in the tropics, and stratospheric O_3 contributes only a few ppbv to tropospheric O_3 column at low latitudes [Roelofs and Lelieveld, 1997]. Therefore, the model analysis suggest that this mid-tropospheric O_3 maximum is caused by African biomass burning emissions of O_3 precursors, possibly

somewhat underestimated by the model due to the neglect of higher hydrocarbon chemistry.

7 Conclusions

A description of the tropospheric O_3 distribution over the Indian Ocean during spring 1995 is presented, and compared to the observations with the nudged ECHAM4 model. This is the first (successful) application of the nudging technique in a chemistry GCM. A number of features present in the O_3 distribution stand out:
- Relatively O_3-deficient air occurs in the marine boundary layer due to efficient photochemical O_3 destruction;
- Relatively high O_3 levels occur close to the Indian continent (~ 20 ppbv) in low-level outflow of polluted air. This is consistent with relatively high CO levels in these air masses.
- Relatively high O_3 levels (~ 15-20 ppbv) are also found at about 20°-30° S, e.g. compared to the central Pacific boundary layer, probably influenced by biomass burning effluents from the African continent.
- Convective outflow in the upper troposphere in the ITCZ causes large-scale O_3 minima over the central Indian Ocean. The vertical extent of the outflow and the O_3 minima is fairly narrow, mostly confined to the 250-100 hPa region.
- At mid-tropospheric levels (750-250 hPa) high O_3 concentrations are apparent, often in confined layers. These high O_3 levels are likely caused by mid-tropospheric outflow of polluted African air, in addition to O_3 that has been transported from the stratosphere.
The ECHAM4 model reproduces the background CO levels as well as the enhanced CO levels in the NHmE and NHcT air masses. The model reproduces the location of these distinct air masses very well. From the comparison between modelled and observed CO it can be concluded that the ECHAM4 model reproduces the large-scale advection processes and the associated tracer transports.

The model reproduces both the overall tendencies and the diurnal variations of the surface pressure, another indication that it simulates the correct meteorology.

Although the model reproduces the spatial O_3 tendencies and relatively low O_3 concentrations compared with O_3 concentrations in the free troposphere, it overestimates O_3 in the marine boundary layer and it underpredicts the diurnal variation in O_3. Since the model underpredicts NO_x over parts of the Indian Ocean, it can be expected that a model increase of O_3 loss is needed rather than a reduction of O_3 production. It is hypothesized that the discrepancy *between the modelled and observed diurnal cycle* is caused by the neglect of multiphase chemistry in clouds or aerosols in the marine boundary layer. Accounting for these processes, e.g. in a future model version, is expected to increase the calculated photochemical O_3 destruction.

The ECHAM4 model reproduces both the upper tropospheric O_3 minima and mid-tropospheric maxima. The model also capable of reproduces the transport of O_3–depleted boundary layer air to the upper troposphere by tropical cyclone Marlene. The upper tropospheric O_3 minimum stretches out over large parts of the Indian Ocean. However, the modelled upper tropospheric O_3 levels are generally too high, consistent with the overestimated surface O_3 levels. On the other hand, the mid-tropospheric O_3 maxima are somewhat underestimated, which could be related to missing higher hydrocarbon chemistry. The mid tropospheric O_3 maxima are caused by transport of polluted air from the southern part of Africa.

Tropical cyclones (e.g. Marlene) influence vertical trace gas distributions over large areas. Organized convection associated with these cyclones enhances vertical exchange between the boundary layer and the free troposphere. Cyclone Marlene caused extended O_3 minima in the middle troposphere and substantially increased the extent of the upper tropospheric O_3 minima.

Future improvements of the model will include implementation of a higher hydrocarbon chemistry scheme to study the role of pollution chemistry in more detail. The model will also be applied at T63 resolution (~ 1.1 x 1.1 degrees) to improve repesentations of synoptic scale weather systems.